ADVANCES IN ATMOSPHERIC SCIENCES, VOL. 35, OCTOBER 2018, 1321–1336

• **Original Paper** •

Circulation Features Associated with the Record-breaking Typhoon Silence in August 2014

Jianpu BIAN[1], Juan FANG[2], Guanghua CHEN*[1], and Chengji LIU[3]

[1]*Center for Monsoon System Research, Institute of Atmospheric Physics, Chinese Academy of Sciences, Beijing* 100026*, China*

[2]*Key Laboratory of Mesoscale Severe Weather (MOE), School of Atmospheric Sciences, Nanjing University, Nanjing* 210023*, China*

[3]*Department of Atmospheric and Oceanic Sciences, University of California, Los Angeles* 90095-1565*, USA*

(Received 21 November 2017; revised 6 March 2018; accepted 2 April 2018)

ABSTRACT

Climatologically, August is the month with the most tropical cyclone (TC) formation over the western North Pacific (WNP) during the typhoon season. In this study, the reason for abnormal TC activity during August is discussed—especially August 2014, when no TCs formed. The large-scale background of August 2014 is presented, with low-level large-scale easterly anomalies and anticyclonic anomalies dominating over the main TC genesis region, a weak monsoon trough system, and a strong WNP subtropical high (WPSH), leading to significantly reduced low-level convergence, upper-level divergence, and mid-level upward motion. These unfavorable large-scale conditions suppressed convection and cyclogenesis. In August 2014, equatorial waves were inactive within the negative phase of the Madden–Julian Oscillation (MJO), with fewer tropical disturbances. Although the low-level vorticity and convection of those disturbances were partly promoted by the convective envelopes of equatorial waves, the integral evolution of disturbances, as well as the equatorial waves, were suppressed when propagating into the negative MJO phase. Moreover, the upper-level potential vorticity (PV) streamers associated with anticyclonic Rossby wave breaking events imported extratropical cold and dry air into the tropics. The peripheral tropospheric dryness and enhanced vertical wind shear by PV streamer intrusion combined with the negative MJO phase were responsible for the absence of TC formation over the WNP in August 2014.

Key words: large-scale pattern, cyclogenesis, MJO, equatorial waves, Rossby wave breaking

Citation: Bian, J. P., J. Fang, G. H. Chen, and C. J. Liu, 2018: Circulation features associated with the record-breaking typhoon silence in August 2014. *Adv. Atmos. Sci.*, **35**(10), 1321–1336, https://doi.org/10.1007/s00376-018-7294-4.

1. Introduction

Tropical cyclones (TCs) are one of the most destructive synoptic systems in the world. The western North Pacific (WNP) is home to the greatest frequency of TC formations, with an annual number of more than 30 (Ching et al., 2010). It is well known that TC formation is largely dependent on the large-scale environmental conditions, which usually require high sea surface temperatures (SSTs), low-level initial cyclonic vorticity, sufficient mid-level humidity, weak vertical wind shear (VWS), and a well-organized deep convective system (Gray, 1968, 1975, 1979). Summer TC genesis over the WNP generally occurs in the warm pool region, in which low-level westerlies over the warm pool converge with the trade easterlies at the southern edge of the WNP subtropical high (WPSH), inducing a southeast–northwest-extending monsoon trough. Most TCs form within the WNP monsoon trough in August, highlighting the crucial role that the monsoon trough plays in TC genesis over the WNP, as stated by McBride (1995) and Ritchie and Holland (1999). Under these favorable large-scale conditions, the timing and location of TC genesis are usually modulated by convectively coupled tropical waves and midlatitude systems.

The role of convectively coupled equatorial waves in TC formation has been extensively discussed in the literature (e.g., Liebmann et al., 1994; Molinari et al., 1997; Maloney and Hartmann, 2000a, 2000b, 2001; Molinari and Vollaro, 2000). It has been found that TCs tend to occur more frequently in the Madden–Julian Oscillation (MJO) convective phase (Liebmann et al., 1994; Straub and Kiladis, 2003; Bessafi and Wheeler, 2006). Kim et al. (2008) further pointed out that the TC frequency increases when the convective MJO envelope dominates over the WNP, and the major TC formation region usually moves along with the propagation of the convective MJO phase during the summertime over the WNP. There is further support that the MJO favors TC genesis by strengthening large-scale low-level convergence and meridional cyclonic shear and inducing an easterly VWS anomaly during the moist phase (Molinari et al., 1997; Maloney

* Corresponding author: Guanghua CHEN
Email: cgh@mail.iap.ac.cn

and Hartmann, 2000b). Other convectively coupled tropical waves can also influence TC genesis by enhancing ascending motion, low-level vorticity, and weakening VWS (Frank and Roundy, 2006; Molinari et al., 2007; Kiladis et al., 2009). For example, TCs frequently develop in association with mixed Rossby–gravity (MRG) waves and tropical depression (TD)-type disturbances over the WNP. Usually acting as predecessors of TD-type disturbances, MRG waves originating from the central and eastern Pacific propagate westward along the equator into the monsoon region over the WNP, and then shift northwestward and transit to TD-type disturbances under the influence of the monsoon trough. Accompanied by a contraction of wavelength and enhancement of wave convection, this transition facilitates tropical cyclogenesis (Dickinson and Molinari, 2002; Aiyyer and Molinari, 2003; Chen and Huang, 2009). Equatorial Rossby (ER) waves promote TC genesis by altering mean flows with low-level convergence and positive vorticity (Molinari et al., 2007; Schreck and Molinari, 2009). Energy analysis also shows that ER waves enhance convergence and easterly wind shear to trap and accumulate energy to promote disturbance development and TC formation (Molinari et al., 2007). Kelvin waves attract less attention than other equatorial waves because previous research has shown that they play a minor role in modulating TC genesis (Frank and Roundy, 2006). However, Schreck (2015) found that cyclogenesis frequently occurs within convective Kelvin wave phases by modulating potential vorticity (PV) and water vapor.

In addition to tropical waves, midlatitude systems, such as upper-level PV streamers associated with Rossby wave breaking (RWB), can also greatly affect TC genesis (Frank and Ritchie, 2001; Galarneau et al., 2015; Zhang et al., 2016, 2017; Bentley et al., 2017). When the mean flows are reduced and the wave's nonlinear amplification is enhanced, RWB tends to take place with the cut-off of upper-level PV streamers from midlatitudes and intrusion of high-PV air into lower latitudes (Thorncroft et al., 1993; Abatzoglou and Magnusdottir, 2006; Liu and Barnes, 2015). However, there is still a debate as to whether upper-level PV streamers play a favorable or unfavorable role in TC development. Some case studies reveal that upper-level PV anomalies on the periphery of the TC would provide a quasi-geostrophic forcing to promote vertical motion (Bosart and Bartlo, 1991). Model results also show that when an upper-level PV anomaly exists above the disturbance, it will promote TC genesis by conducting vertically coupled vortex development and enhancing tropospheric instability, as well as moist convection (Montgomery and Farrell, 1993; Davis and Bosart, 2001, 2003). On the contrary, when midlatitude upper-level PV streamers invade into lower latitudes, those lower-entropy systems with cold and dry air can inhibit moist convection, and thus TC genesis, by enhancing VWS, reducing mid-and-upper tropospheric moisture, and lowering SST as well as tropospheric air temperature (DeMaria et al., 1993; McTaggart-Cowan et al., 2015; Galarneau et al., 2015; Peirano et al., 2016; Zhang et al., 2016, 2017). Moreover, TCs have weaker intensity, shorter life cycles and fewer landfalls when RWB events occur (Zhang et al., 2016, 2017).

Climatologically, August is the month when most TC formations over the WNP occur, with a mean of 5.9 (Fig. 1). However, it is surprising that no TC formed over the WNP in August 2014, which is an unprecedented occurrence among TC records. This intriguing phenomenon motivated us to further investigate the fundamental controlling factors leading to this silence in TC activity in August 2014, based on the large-scale circulation background, tropical waves and midlatitude systems.

Following this introduction, section 2 introduces the data and methods used in the study. In section 3, the climatological anomaly in August 2014 is examined, including the large-scale circulation pattern and genesis potential index (GPI) diagnosis. Section 4 discusses the tropical cyclogenesis associated with the characteristics of the MJO and equatorial waves in August 2014. The influence of midlatitude RWB on tropical cyclogenesis in August 2014 is discussed in section 5. Finally, a summary is presented in section 6.

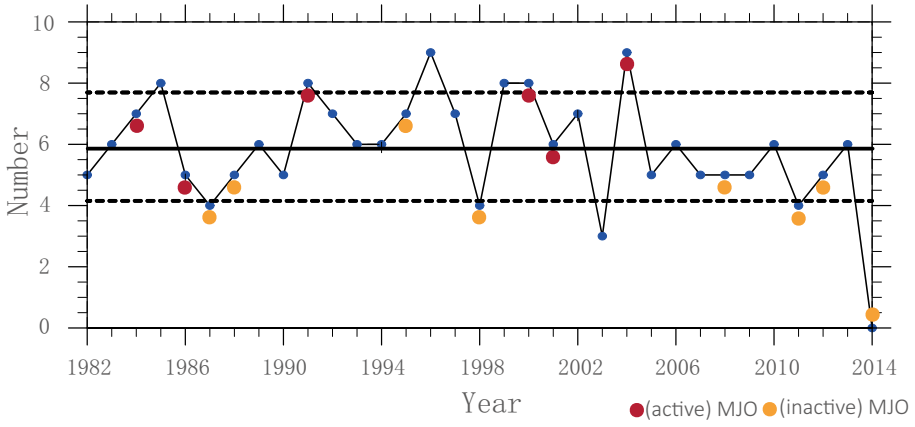

Fig. 1. August TC numbers in the northwestern Pacific from 1982 to 2014. The solid and dashed lines indicate the climatological mean (5.9) and one standard deviation (1.8) of TC counts, respectively. The red (yellow) dots denote the moist (dry) phase of the MJO was situated in the WNP in that year.

2. Data and methods

2.1. *Data*

In this study, the large-scale environmental conditions for TC activity over the WNP in August are described based on the daily and monthly air temperature, wind field, relative and specific humidity, vertical velocity, and SST from the ERA-Interim dataset with a horizontal resolution of 1°. The information on TC genesis over the WNP from 1982 to 2014 is obtained from the Joint Typhoon Warning Center best-track dataset. The TRMM multi-satellite 3B42 precipitation analysis product (Huffman et al., 2007) and daily interpolated outgoing longwave radiation (OLR) (Liebmann, 1996) obtained from NOAA's polar orbiting satellite are used as proxies of deep tropical convection. The grid resolutions of the TRMM and OLR datasets are 0.25° and 2.5°, respectively.

2.2. *Methods*

To further compare the difference in TC activity in August between 2014 and other year groups, the years from 1982 to 2013 are divided into three categories based on TC numbers in August, i.e., TC-active years (1985, 1991, 1996, 1999, 2000 and 2004), TC-inactive years except 2014 (1987, 1998, 2003, 2011), and normal years (Fig. 1). A TC-active (inactive) year is defined as one with more (less) than eight (four) TCs over the WNP in August, which is above (below) the average frequency ($\mu = 5.9$) by one standard deviation ($\sigma = 1.8$).

To explore the key factors inhibiting TC formation over the WNP in August 2014, the GPI proposed by Emanuel and Nolan (2004) and modified by Murakami and Wang (2010) is calculated in this study, expressed as

$$\mathrm{GPI} = |10^5\zeta|^{\frac{3}{2}}\left(\frac{\mathrm{RH}}{50}\right)^3\left(\frac{V_{\mathrm{pot}}}{70}\right)^3(1+0.1V_s)^{-2}\left(\frac{-\omega+0.1}{0.1}\right),$$

where ζ is the 850-hPa absolute vorticity, RH is the 600-hPa relative humidity, V_{pot} is the maximum TC potential intensity (PI, Emanuel, 1995; Bister and Emanuel, 1998), V_s is the magnitude of the VWS (difference between 850 and 200 hPa), and ω is the 500-hPa vertical pressure velocity.

To extract the tropical waves, the wavenumber frequency spectral analysis proposed by Wheeler and Kiladis (1999) is conducted on the TRMM and OLR data in this study. The filtering bands used are similar to those adopted in Schreck et al. (2011, 2012), and Fang and Zhang (2016). The MJO and Kelvin wave bands include 30–90-day and 2.5–17-day periods, as well as eastward propagation at zonal wavenumbers 0–9 and 1–14, respectively. The westward-propagating ER, MRG and TD-type waves cover 9–72-day, 3–10-day and 2.5–5-day periods, and zonal wavenumbers −10 to −1, −10 to −1 and −20 to −6, respectively. In addition, to quantitatively measure the degree of equatorial wave activity, the squared filtered OLR anomalies averaged over (0°–20°N, 120°–180°E) in August, in all 33 years, are normalized. Normalized values larger (smaller) than zero represent activity (inactivity) of equatorial waves.

The MJO activity during August from 1982 to 2014 is examined based on the extensively used real-time multivariate MJO (RMM) index (Wheeler and Hendon, 2004). If the RMM index in August falls within phases 5, 6 or 7 and lasts more than 19 days, it is regarded as an active MJO event. An inactive MJO event has a similar definition except that the RMM index lies in phases 1, 2 or 3. In this way, six active MJO and seven inactive MJO years are identified, which are (1984, 1986, 1991, 2000, 2001 and 2004) and (1987, 1988, 1995, 1998, 2008, 2011 and 2012), respectively.

RWB happens when mean flows are too weak to support the wave's linear propagation and nonlinear amplification is enhanced. There are two irreversible overturning types of RWB, which are termed as either cyclonic (i.e., CWB) or anticyclonic (i.e., AWB), based on the overturning direction (Thorncroft et al., 1993). Previous studies have found that AWB events occur more frequently than CWB ones during boreal summer (Abatzoglou and Magnusdottir, 2006; Strong and Magnusdottir, 2008; Galarneau et al., 2015; Zhang et al., 2016, 2017). Moreover, the accompanying PV streamers associated with AWB always stretch equatorward to lower latitudes during boreal summer, so we only consider AWB events in the North Pacific in this study. According to the detection algorithm of RWB described in Liu and Barnes (2015) and Strong and Magnusdottir (2008), we extract the six-hourly meridional PV gradient reversal of the 2-PVU contour on the 350-K surface (1 PVU = 10^{-6} m^2 s^{-1} K kg^{-1}) to identify AWB events. One AWB occurrence is defined when the reversal happens once, and we detect AWB events from those accumulated occurrences.

3. TC genesis associated with large-scale circulation in August 2014

3.1. *Large-scale patterns in August 2014*

There were 23 TCs formed over the WNP in 2014, which was significantly fewer than the average of 30 TC formations over the WNP. On average, August is considered as the month with the most active TC genesis, whereas it was anomalously silent in August 2014, which was responsible for the relatively low number of TCs in 2014 (Fig. 1). The absence of TC activity in August 2014 broke the existing record held since 1945 over the WNP, and the TC number in this period was more than three standard deviations below the climatological mean number.

A number of previous studies have pointed out that the low-level monsoon trough circulation can significantly modulate summer TC genesis over the WNP (McBride, 1995; Ritchie and Holland, 1999). As shown in Fig. 2a, compared with a normal August, the monsoon trough is stronger and extends more eastward to 150°E in an active-TC August (Fig. 2b). The low-level convergence is comparatively stronger, and the low-level westerly and cyclonic anomalies dominate over the main TC genesis region (TGR, i.e., 5°–25°N, 110°–180°E). In an inactive-TC August, the monsoon trough is much weaker, and large-scale anticyclonic anomalies accompanied by pronounced easterly anomalies dominate over the TGR, providing the unfavorable environmental conditions for

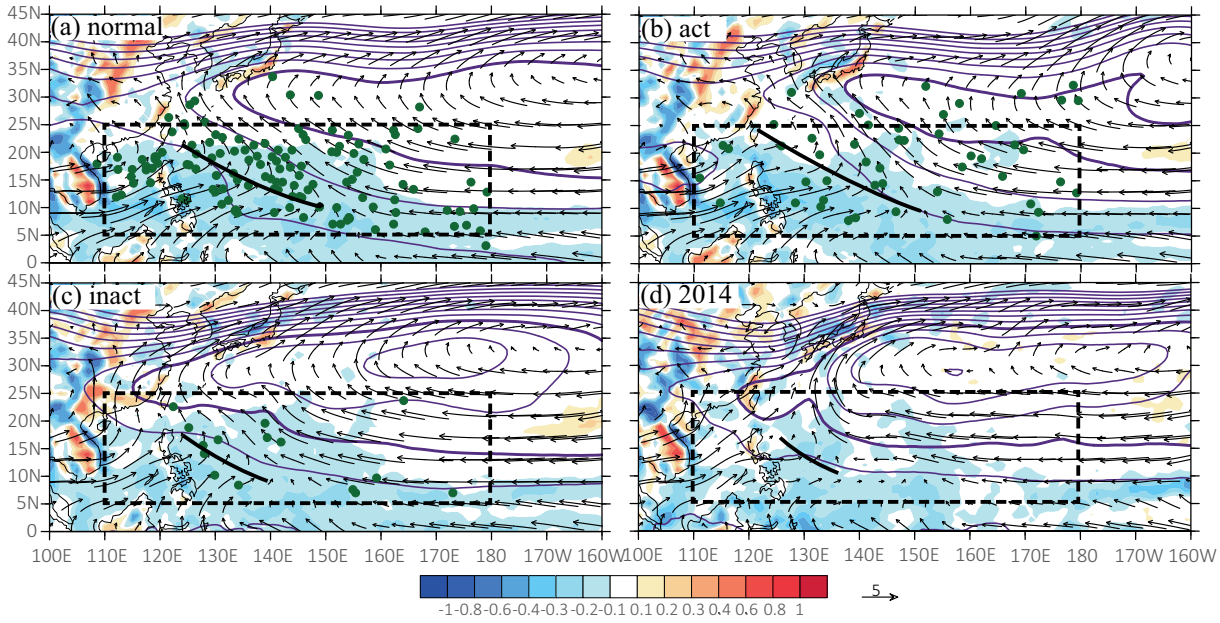

Fig. 2. Composite 850-hPa divergence (shading; units: 10^{-5} s^{-1}), 850-hPa wind fields (vectors), and 500-hPa geopotential height (contours with intervals of 10 gpm) over the WNP for (a) normal August, (b) active-TC August, (c) inactive-TC August, and (d) August 2014. The green dots denote the TC genesis locations. The thick purple contour represents the WPSH (5880 gpm), while the thick black line indicates the monsoon trough. The dashed box (5°–25°N, 110°–180°E) represents the region where TCs are mainly generated in August over the WNP.

tropical cyclogenesis (Figs. 2c and 3c). In contrast to the case in an inactive-TC August, the monsoon trough in August 2014 became much weaker and shrank more westward to around 130°E, inducing strong large-scale anticyclonic anomalies that reinforced the suppression of tropical convection and cyclogenesis in the TGR (Figs. 2d and 3d).

For the mid-and-upper-level system, the WPSH in an active-TC August, represented by the 5880-gpm contour of 500-hPa geopotential height, appears to be weak and shifted more northward than its counterpart in a normal August (cf. Figs. 2a and b), with the westernmost edge located around 140°E, which is more conducive to tropical cyclogenesis combined with an enhanced monsoon trough and low-level convergence (Figs. 2b and 3b). In contrast, during an inactive-TC August, the WPSH becomes robust, featuring a remarkable southwestward extension with the westernmost end of the 5880-gpm contour arriving at 115°E, which produces a low-level divergence anomaly and is thus unfavorable for tropical cyclogenesis (Figs. 2c and 3c). In an active-TC August, positive 200-hPa divergence anomalies are prevalent over the TGR (Figs. 3a and b). The vertical configuration, with strong upper-level divergence and low-level convergence, can produce a TC-friendly environment to facilitate TC development over the TGR. In an inactive-TC August, the 200-hPa divergence demonstrates negative anomalies in the TGR, which is detrimental to tropical convection combined with weakened low-level convergence (Figs. 2c and 3c). Furthermore, this suppressive effect became enhanced in the TGR in August 2014 due to the more vigorous upper-level divergence and greater reduction in low-level convergence (Figs. 2d and 3d).

Tropospheric humidity conditions significantly affect moist convection development, especially for deep convection (e.g., Gray, 1968, 1975; Zhang et al., 2016, 2017). Figure 4 shows the 700–400-hPa precipitable water (PW) anomalies and 500-hPa vertical pressure velocity anomalies in August. In a normal-TC August, mid-tropospheric humidity demonstrates little variation over the TGR (Fig. 4a). In an active-TC August, with the aid of enhanced mid-level vertical motion and large-scale low-level cyclonic anomalies, moist air is brought from the low to the middle level and causes positive mid-tropospheric PW anomalies to dominate over the eastern part of the TGR, which facilitates moist convection development. Meanwhile, reduced mid-level vertical motion and negative low-level cyclonic anomalies dominate over the western part of the TGR, causing negative mid-tropospheric PW anomalies and suppressed moist convection (Figs. 4b and 5b). While negative PW anomalies prevail over the TGR in an inactive-TC August (Fig. 4c), which can exert an unfavorable influence on moist convection accompanied by the reduced mid-level vertical motion and large-scale low-level anticyclonic anomalies. By comparison, in August 2014, both the negative tropospheric moisture anomalies and anomalous mid-level descending motion became much more robust over the TGR, which produced even more pronounced inhibitive conditions for moist convection and tropical cyclogenesis than those in an inactive-TC August (Fig. 4d).

To sum up, in contrast to that in a TC-inactive August, corresponding to the stronger low-level large-scale easterly anomalies and anticyclonic anomalies dominating over the

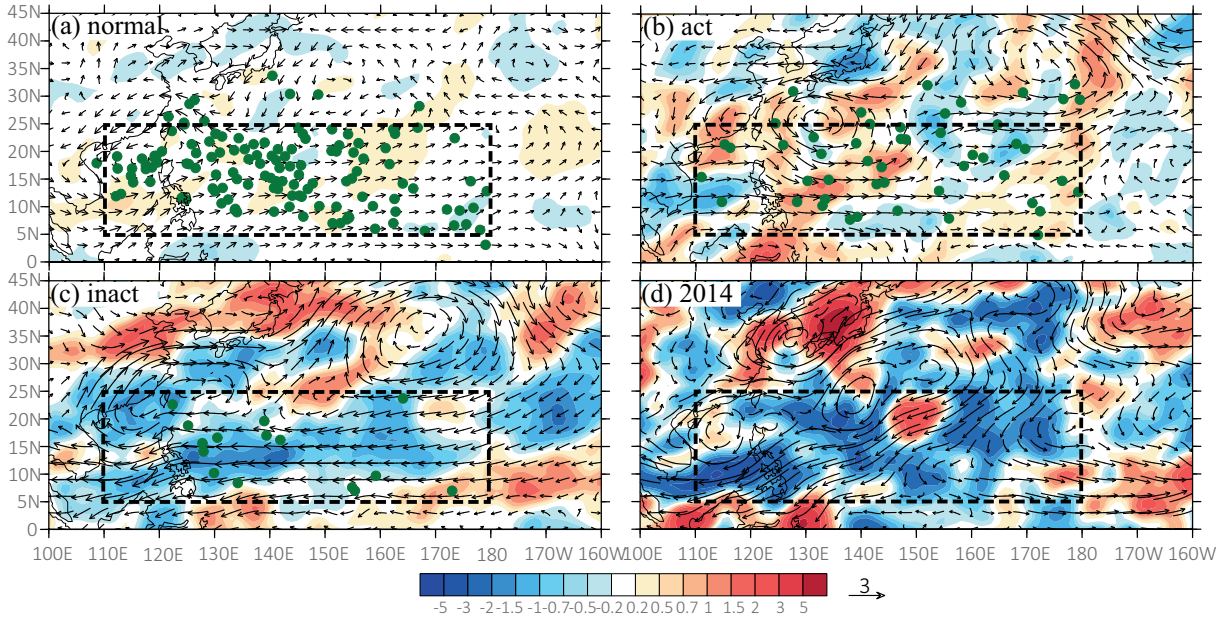

Fig. 3. Composite 200-hPa divergence anomalies (shading; units: 10^{-6} s^{-1}) and 850-hPa wind anomalies (vectors) in (a) normal August, (b) active-TC August, (c) inactive-TC August, and (d) August 2014. The green dots denote the TC genesis locations. The region denoted by the dashed box is the same as that in Fig. 2.

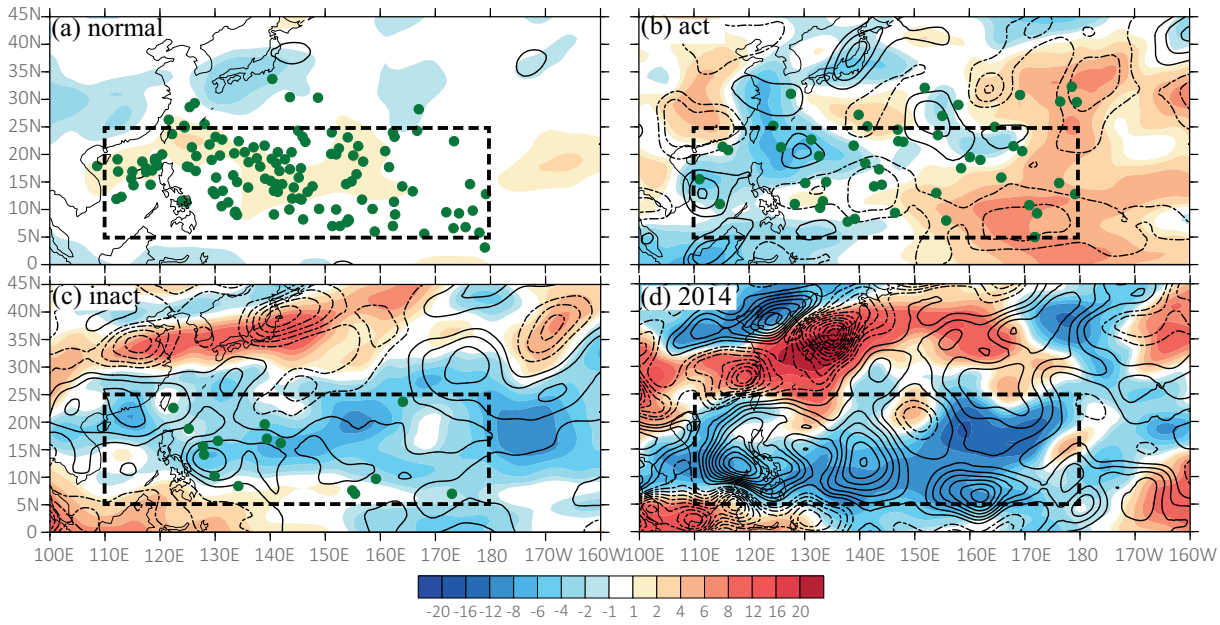

Fig. 4. Composites mid-tropospheric PW anomalies averaged from 700 to 400 hPa (shading; units: mm) and 500-hPa vertical pressure velocity anomalies (contours; every 0.5×10^{-2} Pa s^{-1}; negative is dashed) in (a) normal August, (b) active-TC August, (c) inactive-TC August, and (d) August 2014. The green dots denote the TC genesis locations. The region denoted by the dashed box is the same as that in Fig. 2.

TGR, the circulation in the TGR in August 2014 was characterized by a much weaker low-level cyclonic circulation and monsoon trough system, and a stronger mid-tropospheric WPSH, leading to significantly reduced low-level convergence, upper-level divergence, and mid-level upward motion. It was these unfavorable large-scale conditions that greatly suppressed the convective development, and thus tropical cyclogenesis, in this month.

3.2. *GPI diagnosis in August 2014*

Large-scale background analysis for the month of August has revealed that environmental conditions can significantly

modulate tropical cyclogenesis over the TGR. To understand the key environmental factor or factors leading to the record-breaking TC genesis silence in August 2014, we further examine the individual contribution of five variables comprising the GPI: the low-level vorticity, VWS (850–200 hPa), PI, 600-hPa RH, and ω. Specifically, to explore the contribution of a given variable, the GPI is calculated using the other four variables obtained from the August climatology (1982–2014) and the given variable in August 2014 (Camargo et al., 2007). Figure 5 shows the total GPI anomaly in August 2014 relative to the long-term climatology (Fig. 5a), and the respective contribution from the individual variables (Figs. 5b–f). Negative anomalies of the GPI are observed over the western part of the TGR, while positive anomalies reside over the eastern part (Fig. 5a).

It is evident that the negative GPI anomalies over the TGR to the west of 140°E are mainly attributable to reduced low-level vorticity (Fig. 5b), reduced PI associated with cooler SST (Fig. 5d), enhanced VWS, and descending motion (Figs. 5e and f), which coherently provide unfavorable large-scale conditions for TC genesis. Among the dynamical variations (e.g., low-level vorticity, VWS, and vertical motion), negative descending motion anomalies contribute about 40% of the negative GPI anomalies over the western WNP (5°–25°N, 110°–140°E). Contributions from vorticity, VWS and PI are comparable, accounting for 35%, 12% and 12% of the total GPI change, respectively. Besides, the positive anomalies of GPI are in the eastern section of the TGR, to the east of 140°E. The main contributors to these positive GPI anomalies in this region relate to the reduced VWS (Fig. 5e) and enhanced PI associated with warmer SST in the eastern part of the WNP (Fig. 5d). These results suggest the reduced tropospheric humidity (Fig. 5c) and weakened vertical motion (Fig. 5f) over the TGR may have acted as major inhibiting factors for tropical cyclogenesis in August 2014.

4. Influence of the MJO and equatorial waves on tropical cyclogenesis in August 2014

Tropical waves, such as the MJO, and equatorial waves, can significantly modulate TC genesis. To further examine

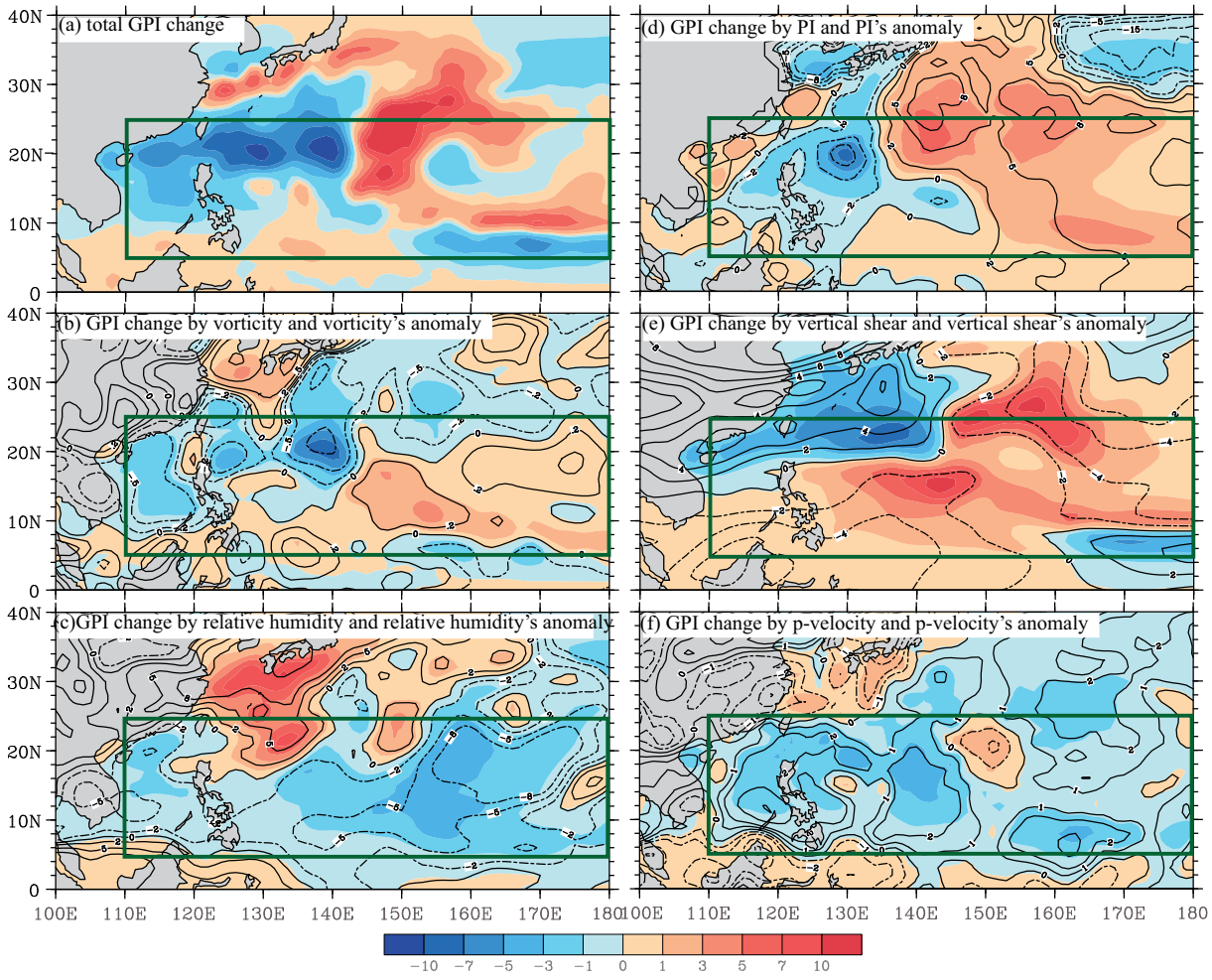

Fig. 5. (a) Total GPI anomaly during August 2014 relative to the August climatology (shading) and the respective contribution from the individual variables (contours; negative is dashed) for (b) 850-hPa vorticity, (c) PI, (d) 600-hPa relative humidity, (e) VWS, and (f) 500-hPa vertical pressure velocity. The green box is similar to Fig. 2.

the underlying mechanisms for no TC occurrence over the WNP in August 2014, the activity of the MJO and equatorial waves, as well as the evolutions of tropical disturbances, are analyzed.

Previous research has shown that the MJO tends to modulate TC genesis significantly over the WNP during the typhoon season (Molinari et al., 1997; Kim et al., 2008). Figure 1 indicates that all the inactive-TC cases occurred during inactive MJO phases, while most of the active-TC cases were associated with active MJO phases, which also suggests the convective MJO phase can favorably promote TC genesis.

As a special case, the evolution of the MJO and convectively-coupled equatorial waves from July to September in 2014 are displayed in Fig. 6. It is clear that July 2014 lay in a convective MJO phase with five TC formations, which was larger than the climatological mean for July. Three TCs were generated within the convective MJO and ER wave phases, one was generated within the convective MJO and Kelvin wave phases, and the other one formed in the active phases of Kelvin waves. Analogous to the conditions in July, six TCs formed in the active MJO phase in September. In sharp contrast, there was no TC genesis in August 2014, in which an anomalously strong MJO dry phase was prevalent over the TGR.

Roundy and Frank (2004) found that relatively high-frequency waves are more significant in the Northern Hemisphere, which can significantly affect tropical cyclogenesis over the WNP. By calculating the standardized squares of area-averaged filtered OLR for each equatorial wave within the negative MJO phase region (5°–30°N, 115°–150°E) in August 2014, those normalized values can represent the degree of wave activity. It clearly displays that all the normalized OLR variance of major equatorial waves were negative in August 2014. In particular, the Kelvin and ER wave values were −0.68 W^2 m^{-4} and −0.57 W^2 m^{-4}, respectively, significantly below the climatological average. The normalized variance of the combined wave was −0.58 W^2 m^{-4}, indicating coherent inactivity of equatorial waves. A number of previous studies have also shown that the MJO can substantially modulate the equatorial waves, as well as TC genesis, during boreal summer (Maloney and Dickinson, 2003; Straub and Kiladis, 2003; Ching et al., 2010; Chen and Chou, 2014). For example, TD-type disturbances are more likely to be enhanced (suppressed) during the active (inactive) MJO phase through the conversion of perturbation kinetic energy between the mean and eddy flows (Maloney and Dickinson,

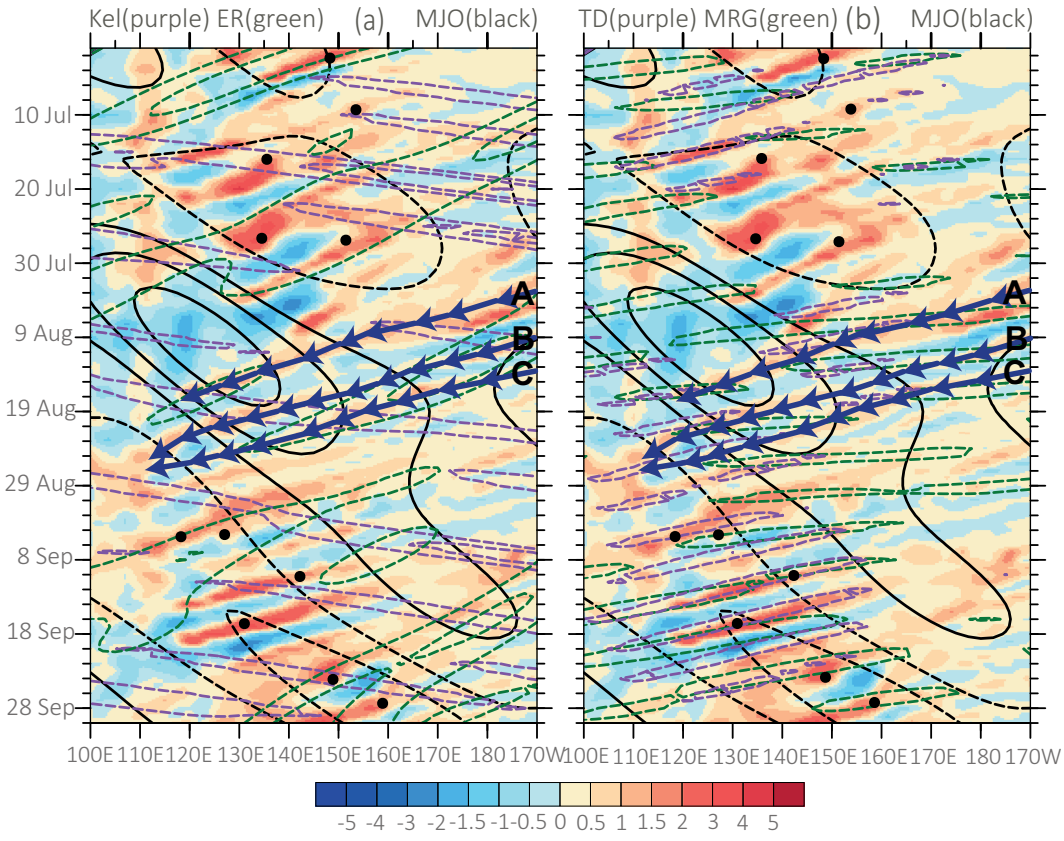

Fig. 6. (a) Longitude–time Hovmöler diagram of 850-hPa vorticity averaged from 2.5°N to 17.5°N (shading; units: 10^{-5} s^{-1}), as well as the MJO-filtered OLR (black contours), ER-filtered OLR (green contours) and Kelvin-filtered OLR (purple contours). (b) Similar to (a) but for the MRG-filtered OLR (green contours) and TD-type-filtered OLR (purple contours). The intervals of the contours are 5 W m^{-2} for the MJO-filtered OLR and 10 W m^{-2} for other wave-filtered OLR. Dots indicate the TC genesis time and location. The deep blue curves with arrows denote the tracks of three tropical disturbances (namely, A, B and C) in August 2014.

2003). MRG waves prefer to transit to vigorous TD disturbances with rapid energy accumulation when propagating westward into the convective MJO phase with a strong flow confluent environment (Aiyyer and Molinari, 2003). ER waves propagate zonally slowly, similar to the speed of MJO phases, allowing the intraseasonal-scale background flow associated with the MJO to fully modulate the ER activity (Kiladis et al., 2009). In turn, ER waves may be tightly coupled with the convective activity of MJO phases, and thus affect the initiation and development of the MJO via the interaction of coupled modes (Kiladis et al., 2009). The triggering of Kelvin waves has an intimate relationship with the MJO, because Kelvin waves partly compose the convective envelope of the MJO during their concomitant propagation, especially over the Indian Ocean (Roundy, 2008). In August 2014, the suppressed phase of the MJO played a key role in the integral inactivity of equatorial waves. The suppressed MJO and inactive equatorial waves were jointly responsible for the below-normal level of TC genesis in August 2014.

Furthermore, careful examination of Fig. 6 shows that there were three coherently westward-propagating tropical disturbances in August 2014, which had a life span of one week or longer, and are labelled A, B and C, respectively. However, those disturbances, as the potential precursors of tropical cyclogenesis, ultimately failed to develop into TCs. Therefore, it would make more sense to examine the evolution characteristics of the three primary disturbances to elucidate the TC silence in this period.

Tropical disturbance A formed in the eastern part of the WNP on 4 August. It began to develop when the disturbance encountered the convective envelopes of ER, MRG and TD-type waves after 6 August (Fig. 7a, and Figs. 8a and b). The convection (represented by the average rainfall) was significantly enhanced by the active phases of the MRG and TD-type waves (Fig. 7a), while the low-level vorticity was partly promoted by the active phase of ER waves (Fig. 7b). After 8 August, the convection of disturbance A was maintained within the convective envelope of TD-type waves, and low-level vorticity was enhanced by the joint active phases of TD-type and ER waves (Figs. 7a and b). Subsequently, disturbance A propagated into the region dominated by the negative phase of the MJO, and the development of disturbance A halted and was then suppressed (Figs. 8d–j). Within the inactive envelope of the MJO, the integral evolution of equatorial waves was also suppressed, contributing less to the development of low-level vorticity and convection of A (Figs. 7a and b). On 16 August, although the active ER and MRG waves contributed positively to convective development, the evolution of A was still suppressed within the strong negative MJO phase. It then began to decay before finally vanishing without

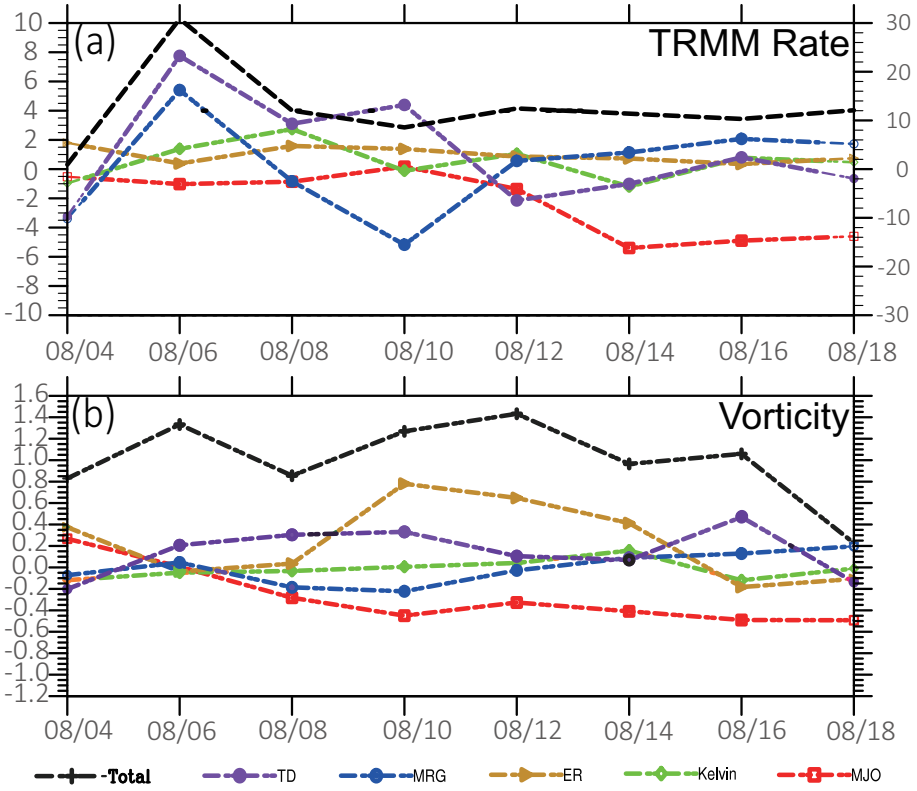

Fig. 7. (a) Temporal evolution of the total TRMM rainfall rate (black lines), MJO-filtered (red), Kelvin-filtered (green), ER-filtered (dark-golden), MRG-filtered (blue) and TD-type-filtered (purple) rainfall averaged in the $10^\circ \times 10^\circ$ domain surrounding the center of disturbance A (units: mm d^{-1}). The scales on the left and right y-axes are for the wave-filtered rainfall and total rainfall, respectively. (b) As in (a) but for the temporal evolution of the total 850-hPa vorticity (units: 10^{-5} s^{-1}).

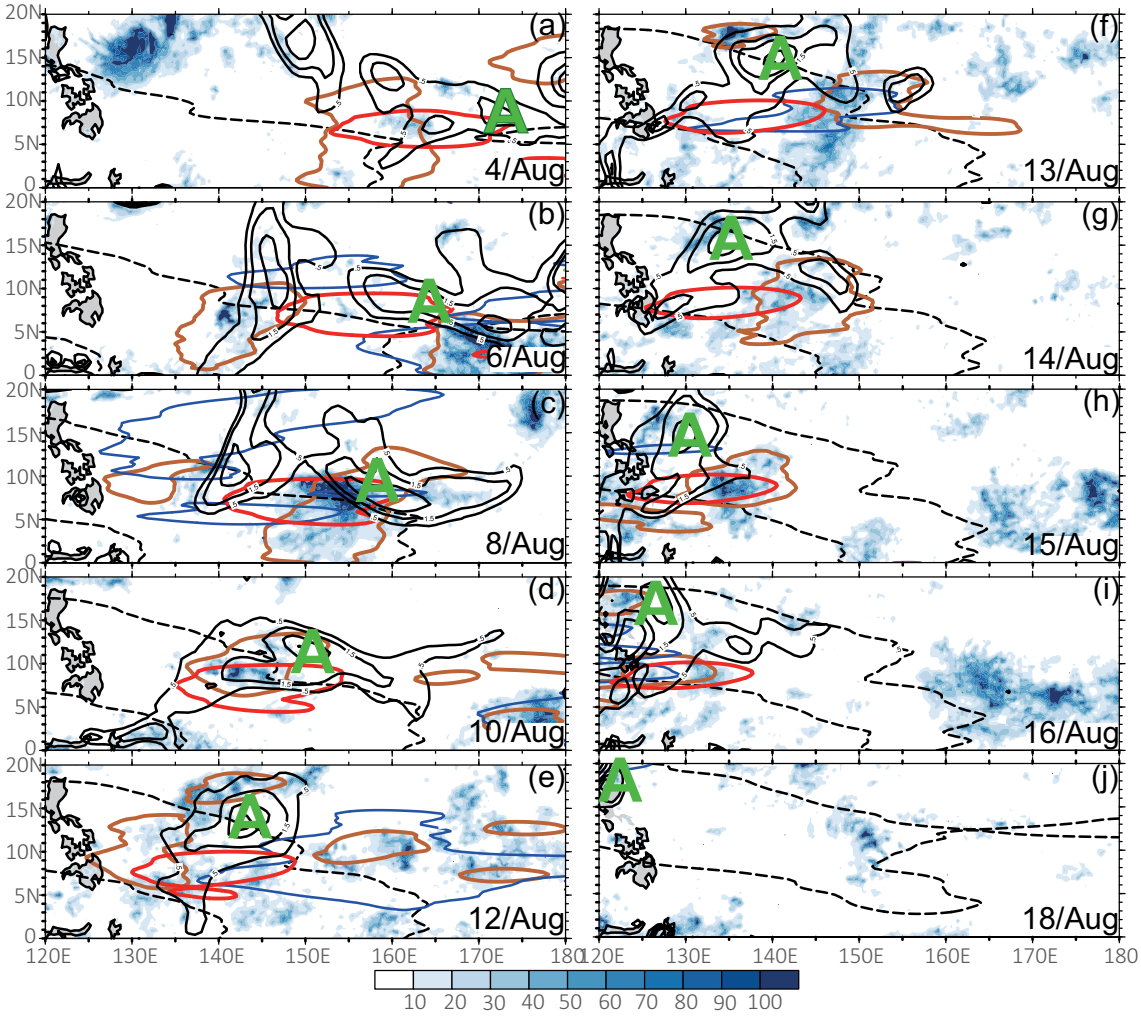

Fig. 8. The relative vorticity (black solid contours above 0.5×10^{-5} s^{-1} with intervals of 10^{-5} s^{-1}) at 850 hPa, as well as the TRMM rainfall rate (shading, units: mm d^{-1}) and MJO-filtered (dashed black contours), ER-filtered (red contours), MRG-filtered (blue contours), and TD-type-filtered (orange contours) rainfall over the WNP corresponding to tropical disturbance A. The contour values are −3 and 3 mm d^{-1} for the MJO signal and 4 mm d^{-1} for the other waves.

developing into a TC.

On 11 August, disturbance B originated to the east of 170°E (Fig. 9a). Combined with the active phases of MRG and ER waves, the low-level vorticity was enhanced (Figs. 9a and b). After 15 August, B propagated into the negative phase of the MJO, and the development of the disturbance was suppressed (Figs. 9d–h). Although active ER, Kelvin and TD-type waves can partly promote convective and low-level vorticity development, the negative MJO phase was detrimental to any further intensification of B (not shown). Subsequently, B propagated westward to merge with disturbance C and developed via the stimulation of active ER waves. However, the effect of tropical waves was insufficient for C to evolve into a TC after leaving the South China Sea.

Disturbance C formed in the eastern WNP within the active phase of ER waves on 14 August (Fig. 10a). With the stimulation of active MRG, TD and ER waves, the convection and low-level vorticity of C were enhanced on 16 August (Fig. 10b). After 18 August, the evolution of C was suppressed when C propagated into the negative MJO phase (Figs. 10d–g). Then, disturbance C combined with B and started to move out of the suppressed MJO phase. It developed rapidly under the influence of active ER waves and TD-type disturbance, with enhanced convection and low-level vorticity (not shown). The large-scale conditions over the western WNP, such as the lower SST, decreased the low-level vorticity and tropospheric humidity, and increased the VWS, were adverse to the development of disturbance C into a TC.

Interestingly, previous research by Yang et al. (2015) also found that the negative phase of intraseasonal oscillation propagated northward into the WNP and inhibited TC genesis in this special month, via enhancing easterlies to induce extratropical dry air and reduce low-level vorticity. However, as with the eastward-propagating intraseasonal oscillation, the MJO did not just provide unfavorable large-scale conditions. In our research, the MJO in this month played more major roles in the lower latitudes and modulated the activity of

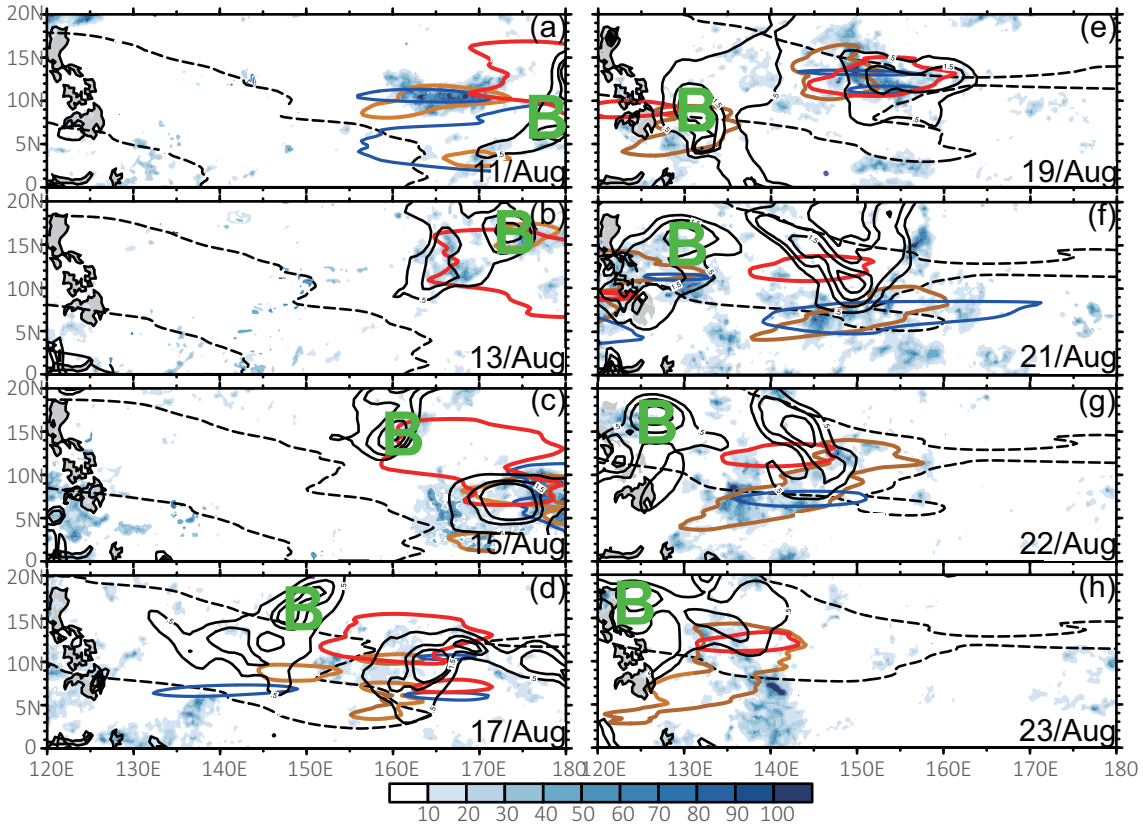

Fig. 9. As in Fig. 8 but for the period from 1200 UTC 11 to 1200 UTC 23 August, corresponding to tropical disturbance B.

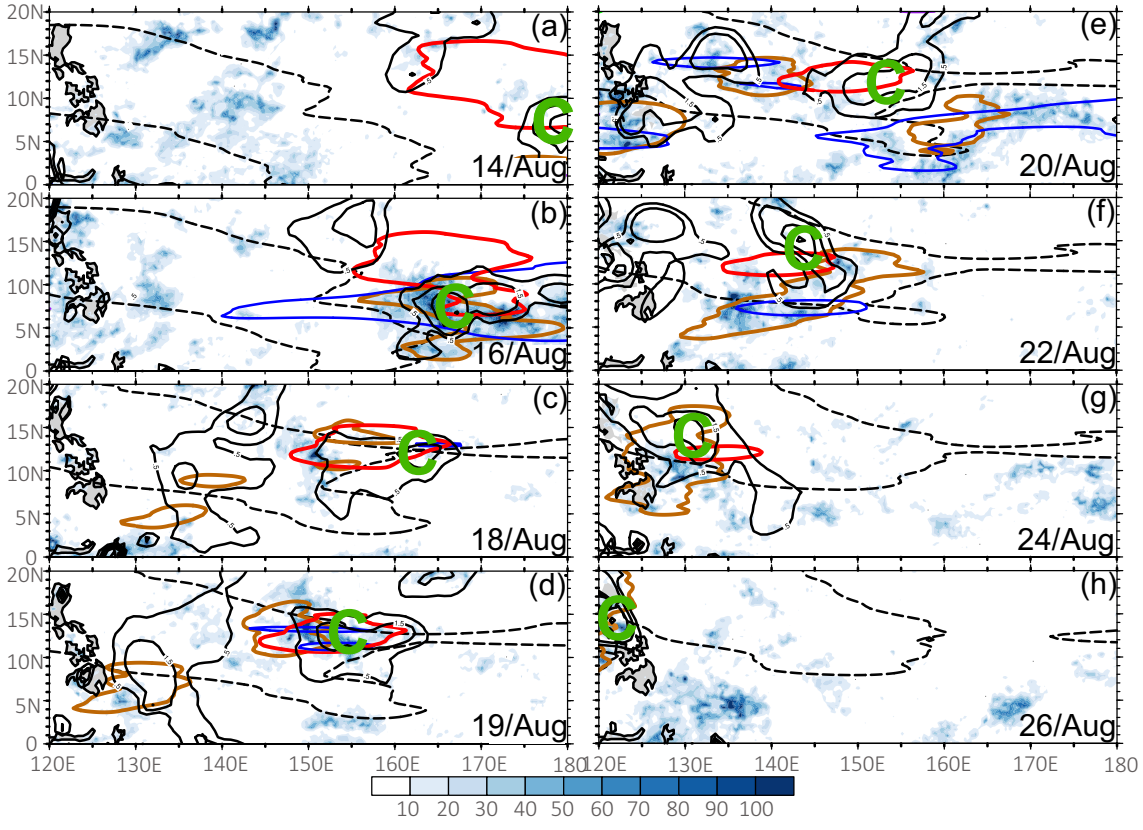

Fig. 10. As in Fig. 8 but for the period from 1200 UTC 14 to 1200 UTC 26 August corresponding to tropical disturbance C.

equatorial waves significantly. Behaving as a multiscale interactive system, the suppressed MJO and inactive equatorial waves were jointly responsible for the fewer tropical disturbances and below-normal TC genesis in August 2014.

5. Influence of AWB on tropical cyclogenesis in August 2014

Other than the large-scale background and tropical systems analyzed above, the midlatitude systems like anticyclonic RWB and extratropical high-PV intrusions can also serve as important factors affecting TC genesis. Previous studies have shown that AWB events frequently induce upper-level PV streamers to overturn southward to lower latitudes (Thorncroft et al., 1993; Zhang et al., 2016). Those PV streamers cause intrusions of cold and dry air into the tropics, which provide unfavorable large-scale conditions to suppress moist convection and TC development, by reducing tropospheric moisture, enhancing VWS, and lowering SSTs (Galarneau et al., 2015; Zhang et al., 2016, 2017).

To give a further interpretation of upper-level PV streamers associated with AWB processes, we select several AWB events during the evolutions of tropical disturbances in August 2014. We examine the tropospheric conditions in this month by analyzing the PV on the 350-K isentropic surface, the 850–200-hPa thickness (THK), and tropospheric PW averaged from 850 to 200 hPa.

Figures 11–13 show the several AWB events and associated large-scale circulation evolutions in August 2014. Before 0000 UTC 12 August, an AWB event occurred to the northeast of the WNP, inducing the accompanying upper-level PV streamer to propagate southwestward into the lower latitudes. Then, the PV streamer located on the northeast-

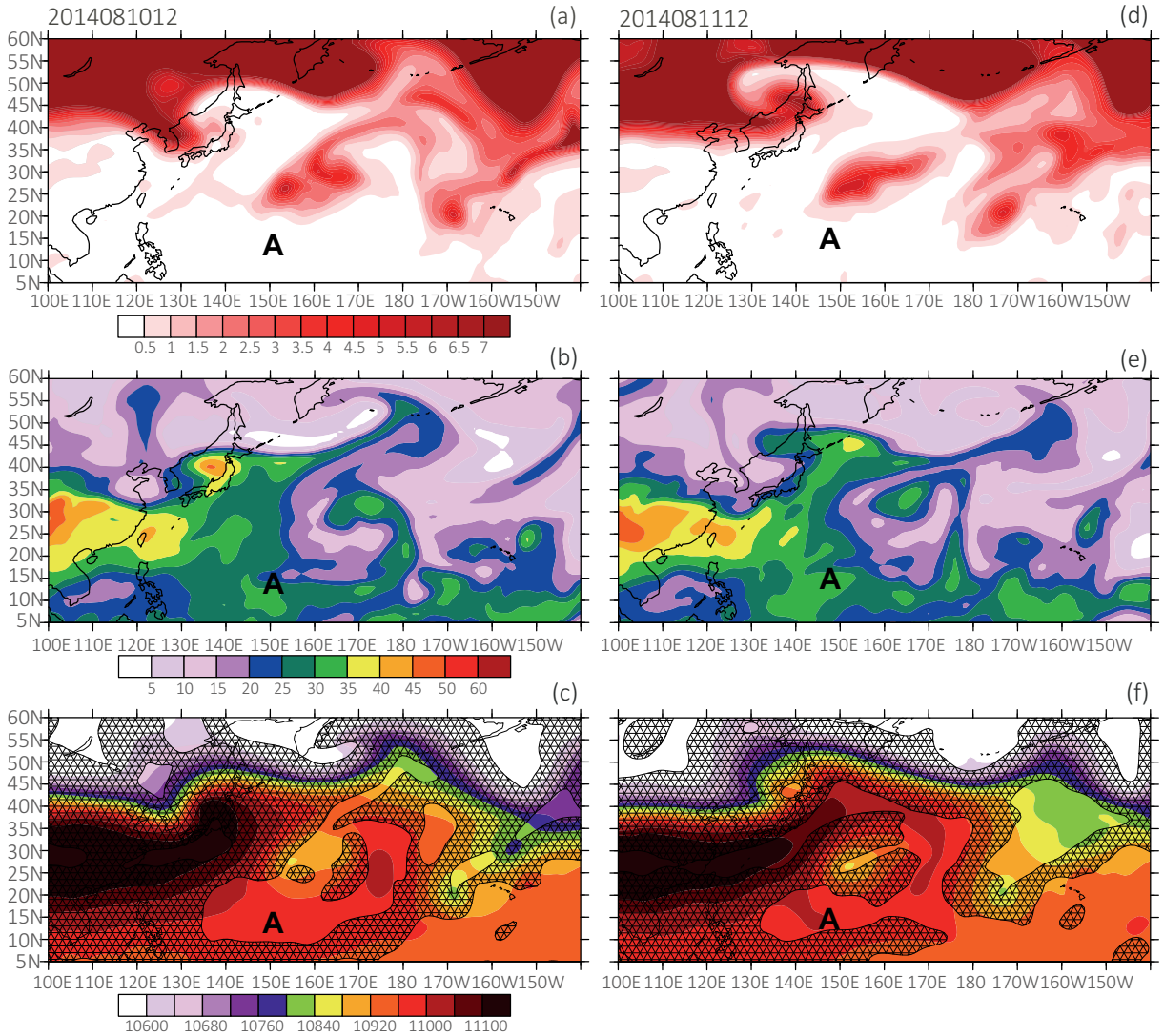

Fig. 11. Horizontal plane view of the 350-K isentropic PV (shading; units: 1 PVU) over the WNP at (a) 0000 UTC 12 and (d) 0000 UTC 13 August 2014. (b, e) As in (a, d) but for PW (units: mm). (c, f) As in (a, d) but for THK (units: m) and 200–850-hPa VWS (hatched areas > 12 m s^{-1}). The label "A" represents the location of the first tropical disturbance in August 2014.

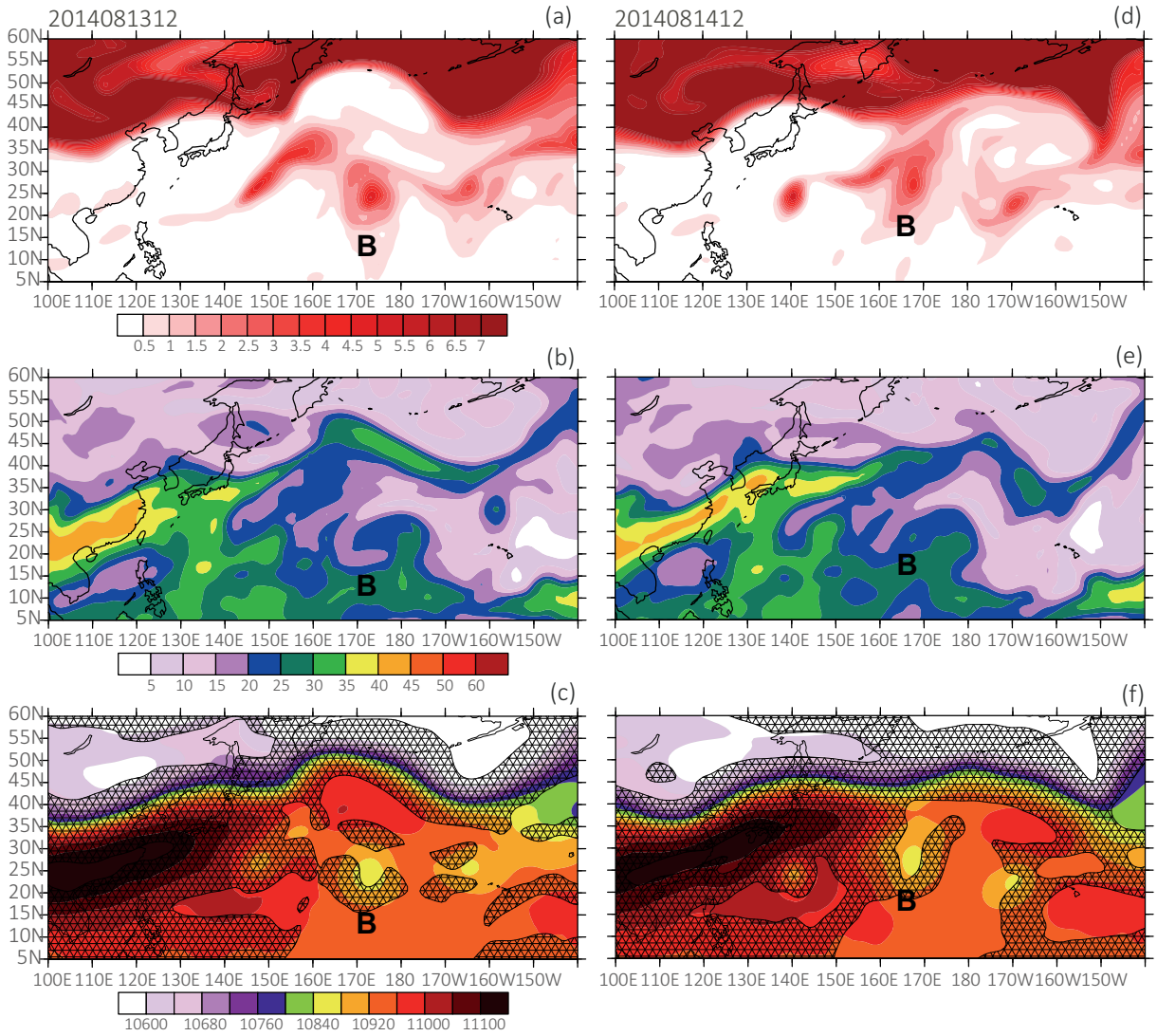

Fig. 12. As in Fig. 11 but for the period from 1200 UTC 13 to 1200 UTC 14 August. The label "B" represents the location of the second analyzed tropical disturbance in August 2014.

ern flank of tropical disturbance A began to move westward along with disturbance A. During the stagnation in the tropics, the PV streamer was stretched and formed a cut-off low (Fig. 11a). As an extratropical low entropy system, the cut-off low brought dry air to lower latitudes to reduce the peripheral tropospheric humidity on the eastern flank of A (Figs. 11b and e). Besides, the cut-off low had a cold tongue accompanied by lower THK that enhanced the temperature gradient between the PV streamer and A, causing the strong VWS due to thermal wind balance (Fig. 11c). At 0000 UTC 13 August, A was located at (13.5°N, 146°E), beneath the cut-off low (Fig. 11d). The temperature gradient became sharp and dense to contribute to the strong VWS between the cut-off low and A (Fig. 11f). The unfavorable large-scale environments inhibited the development of moist convection and cyclogenesis.

After the AWB event occurred, the accompanying upper-level PV streamer moved southwestward into the periphery of tropical disturbance B from 1200 UTC 13 August (Figs. 12a and d). Extratropical dry air intrusion accompanied by the low PW reduced the tropospheric humidity on the northern flank of B (Figs. 12b and e), which also contributed to the cold temperature anomalies and enhanced the VWS in the periphery of the disturbance (Figs. 12c and f). After 1200 UTC 14 August, B moved westward to 165°E (Fig. 12d). The VWS was enhanced when B was stretched closer to the southern flank of the PV streamer and ambient tropospheric humidity became dry, causing the unfavorable conditions for moist convection development and TC genesis (Figs. 12e and f). In addition, another AWB event occurred to the east of the date line after 1200 UTC 17 August. The upper-level PV streamer approached tropical disturbance C from the southwest (Figs. 13a, 13d). The dry and cold air associated with the PV streamer reduced the peripheral tropospheric humidity and enhanced the VWS on the northern and eastern flanks of C, which suppressed the moist convection and prevented

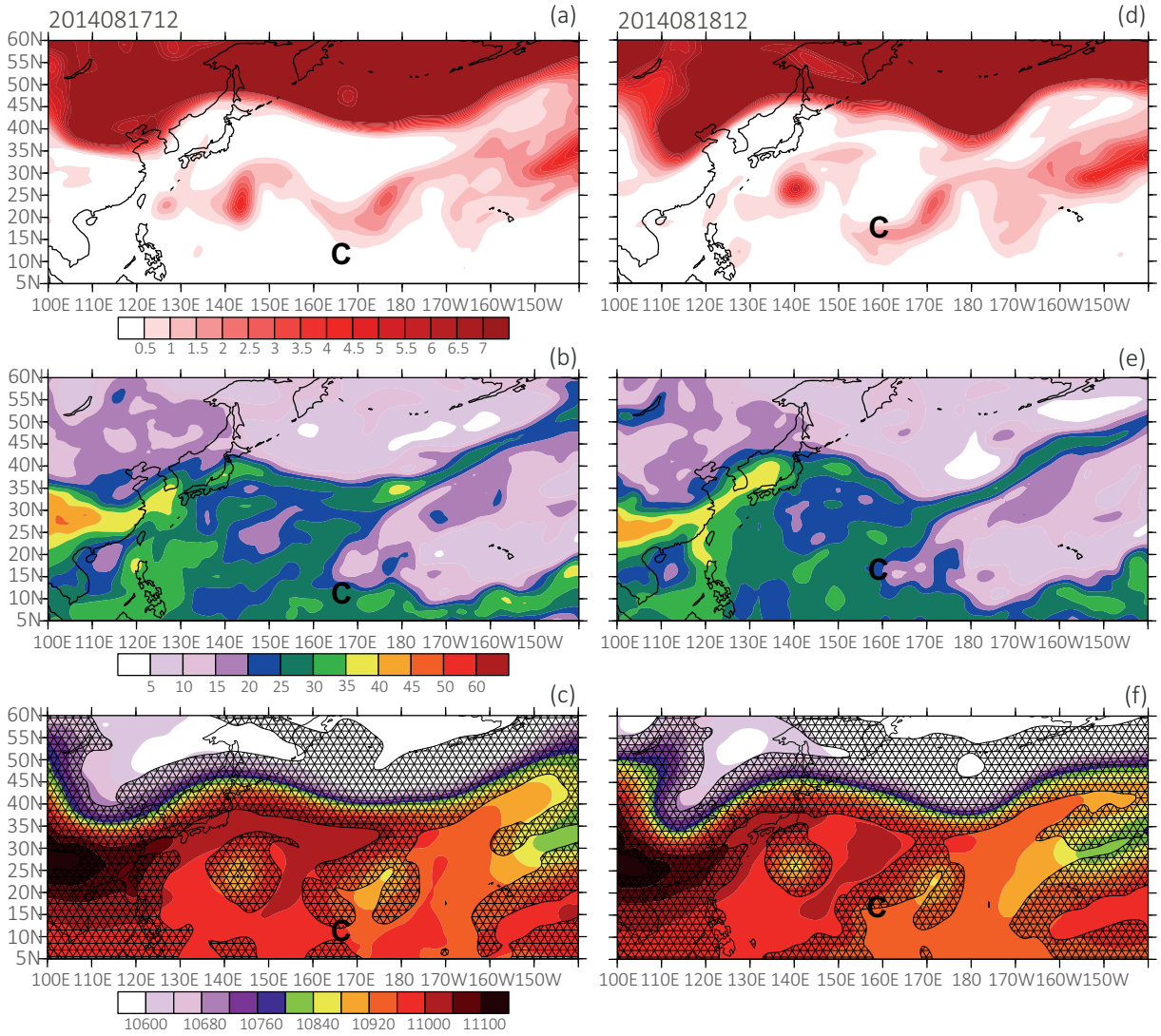

Fig. 13. As in Fig. 11 but for the period from 1200 UTC 17 to 1200 UTC 18 August. The label C represents the location of the third analyzed tropical disturbance in August 2014.

the disturbance from developing into a TC (Figs. 13b and e; Figs. 13c and f).

In summary, other than the influence of the equatorial waves within the inactive MJO phase in August 2014, extratropical PV intrusions associated with AWB events that reduced the ambient humidity and enhanced the VWS may also have significantly suppressed the development of convection and thus inhibited those disturbances from evolving into TCs.

6. Summary

Climatologically, frequent TC activity over the WNP is expected in August. However, in an unprecedented phenomenon, no TC formation took place in August 2014. Based on analysis of the climatological background for the month of August, significant differences in the large-scale patterns were found to exist at different tropospheric levels during periods of relatively less or more TC occurrence at this time. In an August with inactive TC genesis, the main TGR is dominated by a weak monsoon trough and low-level anticyclonic anomalies associated with easterly anomalies. Moreover, a stronger mid-level WPSH and more reduced upper-level divergence, as well as drier mid-tropospheric humidity, prevail over the TGR in a TC-inactive August compared with a TC-active August. Those unfavorable large-scale conditions suppress moist convection and tropical cyclogenesis. When those large-scale conditions in August become adverse, TC genesis is active in the TGR. In contrast to the cases in other years, in August 2014, the monsoon trough and upper-level divergence were weaker, while the mid-level WPSH was stronger. Smaller mid-tropospheric moisture, stronger low-level anticyclonic circulation and easterly anomalies, and reduced mid-level vertical motion, dominated in the TGR, suppressing the development of convection and cyclogenesis. Further GPI diagnosis revealed that reduced tropospheric

humidity and mid-level vertical motion over the TGR had an important influence on the cyclogenesis silence in this special month.

The MJO plays an important role in modulating the equatorial waves and TC genesis in August. The suppressive phase of the MJO was a main contributor to the inactivity of equatorial waves in August 2014. All the normalized OLR variance of major equatorial waves was negative in this month, especially for the Kelvin and ER waves, with values significantly below the climatological average. Moreover, fewer tropical disturbances associated with the integral inactivity of equatorial waves emerged in August 2014. Although the low-level vorticity and convection of those disturbances were partly promoted by the convective envelopes of equatorial waves in the eastern part of the WNP, the integral development was suppressed when the disturbances propagated into the negative MJO phase and was less likely to amplify.

Extratropical systems also played an important role in modulating the evolution of tropical disturbances and cyclogenesis in August 2014. AWB events occurred on the northern and northeastern flanks of disturbances, inducing upper-level PV streamers to penetrate southwestward into the lower latitudes. During stagnation in the tropics, the upper-level PV streamers brought extratropical cold and dry air to reduce the ambient tropospheric humidity on the northern and eastern flanks of disturbances. The cold tongue associated with PV streamers lowered the THK and enhanced temperature gradient between the streamers and disturbances, causing strong VWS in response to thermal wind balance. Eventually, the joint contribution of the negative phase of the MJO, the integral inactivity of equatorial waves, and the tropospheric low-entropy air intrusion and enhanced VWS related to the AWB and PV streamers, led to the TC silence in August 2014.

Acknowledgements. We thank Dr. Haikun ZHAO and Dr. Pinhong HUI for their constructive comments on our research. This work was supported by the National Natural Science Foundation of China (Grant Nos. 41475074, 41775063 and 41475046).

REFERENCES

Abatzoglou, J. T., and G. Magnusdottir, 2006: Planetary wave breaking and nonlinear reflection: Seasonal cycle and interannual variability. *J. Climate*, **19**(23), 6139–6152, https://doi.org/10.1175/JCLI3968.1.

Aiyyer, A. R., and J. Molinari, 2003: Evolution of mixed Rossby–gravity waves in idealized MJO environments. *J. Atmos. Sci.*, **60**(23), 2837–2855, https://doi.org/10.1175/1520-0469(2003)060<2837:EOMRWI>2.0.CO;2.

Bentley, A. M., L. F. Bosart, and D. Keyser, 2017: Upper-tropospheric precursors to the formation of subtropical cyclones that undergo tropical transition in the North Atlantic basin. *Mon. Wea. Rev.*, **145**(2), 503–520, https://doi.org/10.1175/MWR-D-16-0263.1.

Bessafi, M., and M. C. Wheeler, 2006: Modulation of South Indian Ocean tropical cyclones by the Madden-Julian oscillation and convectively coupled equatorial waves. *Mon. Wea. Rev.*, **134**(2), 638–656, https://doi.org/10.1175/MWR3087.1.

Bister, M., and K. A. Emanuel, 1998: Dissipative heating and hurricane intensity. *Meteor. Atmos. Phys.*, **65**(3–4), 233–240, https://doi.org/10.1007/BF01030791.

Bosart, L. F., and J. A. Bartlo, 1991: Tropical storm formation in a baroclinic environment. *Mon. Wea. Rev.*, **119**(8), 1979–2013, https://doi.org/10.1175/1520-0493(1991)119<1979:TSFIAB>2.0.CO;2.

Camargo, S. J., K. A. Emanuel, and A. H. Sobel, 2007: Use of a genesis potential index to diagnose ENSO effects on tropical cyclone genesis. *J. Climate*, **20**(19), 4819–4834, https://doi.org/10.1175/JCLI4282.1.

Chen, G. H., and C. Chou, 2014: Joint contribution of multiple equatorial waves to tropical cyclogenesis over the western North Pacific. *Mon. Wea. Rev.*, **142**(1), 79–93, https://doi.org/10.1175/MWR-D-13-00207.1.

Chen, G. H., and R. H. Huang, 2009: Interannual variations in mixed Rossby-gravity waves and their impacts on tropical cyclogenesis over the western North Pacific. *J. Climate*, **22**(3), 535–549, https://doi.org/10.1175/2008JCLI2221.1.

Ching, L., C. H. Sui, and M. J. Yang, 2010: An analysis of the multiscale nature of tropical cyclone activities in June 2004: Climate background. *J. Geophys. Res.*, **115**(D24), D24108, https://doi.org/10.1029/2010JD013803.

Davis, C. A., and L. F. Bosart, 2001: Numerical simulations of the genesis of Hurricane Diana (1984). Part I: Control simulation. *Mon. Wea. Rev.*, **129**(8), 1859–1881, https://doi.org/10.1175/1520-0493(2001)129<1859:NSOTGO>2.0.CO;2.

Davis, C. A., and L. F. Bosart, 2003: Baroclinically induced tropical cyclogenesis. *Mon. Wea. Rev.*, **131**(11), 2730–2747, https://doi.org/10.1175/1520-0493(2003)131<2730:BITC>2.0.CO;2.

DeMaria, M., J.-J. Baik, and J. Kaplan, 1993: Upper-level eddy angular momentum fluxes and tropical cyclone intensity change. *J. Atmos. Sci.*, **50**(8), 1133–1147, https://doi.org/10.1175/1520-0469(1993)050<1133:ULEAMF>2.0.CO;2.

Dickinson, M., and J. Molinari, 2002: Mixed Rossby–gravity waves and western Pacific tropical cyclogenesis. Part I: Synoptic evolution. *J. Atmos. Sci.*, **59**(14), 2183–2196, https://doi.org/10.1175/1520-0469(2002)059<2183:MRGWAW>2.0.CO;2.

Emanuel, K. A., 1995: Sensitivity of tropical cyclones to surface exchange coefficients and a revised steady-state model incorporating eye dynamics. *J. Atmos. Sci.*, **52**(22), 3969–3976, https://doi.org/10.1175/1520-0469(1995)052<3969:SOTCTS>2.0.CO;2.

Emanuel, K. A., and D. S. Nolan, 2004: Tropical cyclone activity and the global climate system. *Preprints, 26th Conf. on Hurricanes and Tropical Meteorology*, Miami, FL, Amer. Meteor. Soc. A., 10 pp.

Fang, J., and F. Q. Zhang, 2016: Contribution of tropical waves to the formation of super typhoon Megi (2010). *J. Atmos. Sci.*, **73**, 4387–4405, https://doi.org/10.1175/JAS-D-15-0179.1.

Frank, W. M., and E. A. Ritchie, 2001: Effects of vertical wind shear on the intensity and structure of numerically simulated hurricanes. *Mon. Wea. Rev.*, **129**(9), 2249–2269, https://doi.org/10.1175/1520-0493(2001)129<2249:EOVWSO>2.0.CO;2.

Frank, W. M., and P. E. Roundy, 2006: The role of tropical waves in tropical cyclogenesis. *Mon. Wea. Rev.*, **134**(9), 2397–2417, https://doi.org/10.1175/MWR3204.1.

Galarneau, T. J., Jr., R. McTaggart-Cowan, L. F. Bosart, and C. A. Davis, 2015: Development of North Atlantic tropical dis-

turbances near upper-level potential vorticity streamers. *J. Atmos. Sci.*, **72**(2), 572–597, https://doi.org/10.1175/JAS-D-14-0106.1.

Gray, W. M., 1968: Global view of the origin of tropical disturbances and storms. *Mon. Wea. Rev.*, **96**(10), 669–700, https://doi.org/10.1175/1520-0493(1968)096<0669:GVOTOO>2.0.CO;2.

Gray, W. M., 1975: Tropical Cyclone Genesis in the Western North Pacific. Department of Atmospheric Science, Colorado State University, Fort Collins, Colorado.

Gray, W. M., 1979: Hurricanes: Their formation, structure and likely role in the tropical circulation. *Meteorology over the Tropical Oceans*, **77**, 155–218.

Huffman, G. J., D. T. Bolvin, E. J. Nelkin, and D. B. Wolff, 2007: The TRMM multisatellite precipitation analysis (TMPA): Quasi-global, multiyear, combined-sensor precipitation estimates at fine scales. *Journal of Hydrometeorology*, **8**(1), 38–55, https://doi.org/10.1175/JHM560.1.

Kiladis, G. N., M. C. Wheeler, P. T. Haertel, K. H. Straub, and P. E. Roundy, 2009: Convectively coupled equatorial waves. *Rev. Geophys.*, **47**(2), RG2003, https://doi.org/10.1029/2008RG000266.

Kim, J.-H., C.-H. Ho, H.-S. Kim, C.-H. Kim, and S. K. Park, 2008: Systematic variation of summertime tropical cyclone activity in the western North Pacific in relation to the Madden-Julian oscillation. *J. Climate*, **21**(6), 1171–1191, https://doi.org/10.1175/2007JCLI1493.1.

Liebmann, B., 1996: Description of a complete (interpolated) outgoing longwave radiation dataset. *Bull. Amer. Meteor. Soc.*, **77**, 1275–1277.

Liebmann, B., H. Hendon, and J. D. Glick, 1994: The relationship between tropical cyclones of the western Pacific and Indian Oceans and the Madden–Julian oscillation. *J. Meteor. Soc. Japan*, **72**(3), 401–412, https://doi.org/10.2151/jmsj1965.72.3_401.

Liu, C. J., and E. A. Barnes, 2015: Extreme moisture transport into the Arctic linked to Rossby wave breaking. *J. Geophys. Res.*, **120**(9), 3774–3788, https://doi.org/10.1002/2014JD022796.

Maloney, E. D., and D. L. Hartmann, 2000a: Modulation of eastern North Pacific hurricanes by the Madden–Julian oscillation. *J. Climate*, **13**(9), 1451–1460, https://doi.org/10.1175/1520-0442(2000)013<1451:MOENPH>2.0.CO;2.

Maloney, E. D., and D. L. Hartmann, 2000b: Modulation of hurricane activity in the Gulf of Mexico by the Madden–Julian oscillation. *Science*, **287**(5460), 2002–2004, https://doi.org/10.1126/science.287.5460.2002.

Maloney, E. D., and D. L. Hartmann, 2001: The Madden-Julian oscillation, barotropic dynamics, and north pacific tropical cyclone formation. Part I: Observations. *Journal of Atmospheric Sciences*, **58**, 2545–2558, https://doi.org/10.1175/1520-0469(2001)058<2545:TMJOBD>2.0.CO;2.

Maloney, E. D., and M. J. Dickinson, 2003: The intraseasonal oscillation and the energetics of summertime tropical western North Pacific synoptic-scale disturbances. *J. Atmos. Sci.*, **60**(17), 2153–2168, https://doi.org/10.1175/1520-0469(2003)060<2153:TIOATE>2.0.CO;2.

McBride, J. L., 1995: Tropical cyclone formation. Chapter 3,. *Global Perspectives on Tropical Cyclones*, R. L. Elsberry, Ed., Tech. Doc. WMO/TD No. 693, World Meteorological Organization, Geneva, Switzerland, 63–105.

McTaggart-Cowan, R., E. L. Davies, J. G. Fairman, Jr., T. J. Galarneau, Jr., and D. M. Schultz, 2015: Revisiting the 26.5° sea surface temperature threshold for tropical cyclone development. *Bull. Amer. Meteor. Soc.*, **96**(11), 1929–1943, https://doi.org/10.1175/BAMS-D-13-00254.1.

Molinari, J., and D. Vollaro, 2000: Planetary-and synoptic-scale influences on eastern Pacific tropical cyclogenesis. *Mon. Wea. Rev.*, **128**(9), 3296–3307, https://doi.org/10.1175/1520-0493(2000)128<3296:PASSIO>2.0.CO;2.

Molinari, J., D. Knight, M. Dickinson, D. Vollaro, and S. Skubis, 1997: Potential vorticity, easterly waves, and eastern Pacific tropical cyclogenesis. *Mon. Wea. Rev.*, **125**(10), 2699–2708, https://doi.org/10.1175/1520-0493(1997)125<2699:PVEWAE>2.0.CO;2.

Molinari, J., K. Lombardo, and D. Vollaro, 2007: Tropical cyclogenesis within an equatorial Rossby wave packet. *J. Atmos. Sci.*, **64**(4), 1301–1317, https://doi.org/10.1175/JAS3902.1.

Montgomery, M. T., and B. F. Farrell, 1993: Tropical cyclone formation. *J. Atmos. Sci.*, **50**(2), 285–310, https://doi.org/10.1175/1520-0469(1993)050<0285:TCF>2.0.CO;2.

Murakami, H., and B. Wang, 2010: Future change of north atlantic tropical cyclone tracks: Projection by a 20-Km-mesh global atmospheric model. *J. Climate*, **23**(10), 2699–2721, https://doi.org/10.1175/2010JCLI3338.1.

Peirano, C. M., K. L. Corbosiero, and B. H. Tang, 2016: Revisiting trough interactions and tropical cyclone intensity change. *Geophys. Res. Lett.*, **43**(10), 5509–5515, https://doi.org/10.1002/2016GL069040.

Ritchie, E. A., and G. J. Holland, 1999: Large-scale patterns associated with tropical cyclogenesis in the western Pacific. *Mon. Wea. Rev.*, **127**(9), 2027–2043, https://doi.org/10.1175/1520-0493(1999)127<2027:LSPAWT>2.0.CO;2.

Roundy, P. E., and W. M. Frank, 2004: A climatology of waves in the equatorial region. *J. Atmos. Sci.*, **61**(17), 2105–2132, https://doi.org/10.1175/1520-0469(2004)061<2105:ACOWIT>2.0.CO;2.

Roundy, P. E., 2008: Analysis of convectively coupled Kelvin waves in the Indian Ocean MJO. *J. Atmos. Sci.*, **65**(4), 1342–1359, https://doi.org/10.1175/2007JAS2345.1.

Schreck, C. J., III, and J. Molinari, 2009: A case study of an outbreak of twin tropical cyclones. *Mon. Wea. Rev.*, **137**(3), 863–875, https://doi.org/10.1175/2008MWR2541.1.

Schreck C. J., III, 2015: Kelvin waves and tropical cyclogenesis: A global survey. *Mon. Wea. Rev.*, **143**(10), 3996–4011, https://doi.org/10.1175/MWR-D-15-0111.1.

Schreck, C. J., III, J. Molinari, and K. I. Mohr, 2011: Attributing tropical cyclogenesis to equatorial waves in the western North Pacific. *J. Atmos. Sci.*, **68**(2), 195-209, https://doi.org/10.1175/2010JAS3396.1.

Schreck, C. J., III, J. Molinari, and A. Aiyyer, 2012: A global view of equatorial waves and tropical cyclogenesis. *Mon. Wea. Rev.*, **140**(3), 774–788, https://doi.org/10.1175/MWR-D-11-00110.1.

Straub, K. H., and G. N. Kiladis, 2003: Interactions between the boreal summer intraseasonal oscillation and higher-frequency tropical wave activity. *Mon. Wea. Rev.*, **131**(5), 945–960, https://doi.org/10.1175/1520-0493(2003)131<0945:IBTBSI>2.0.CO;2.

Strong, C., and G. Magnusdottir, 2008: Tropospheric Rossby wave breaking and the NAO/NAM. *J. Atmos. Sci.*, **65**(9), 2861-2876, https://doi.org/10.1175/2008JAS2632.1.

Thorncroft, C. D., B. J. Hoskins, and M. E. McIntyre, 1993: Two paradigms of baroclinic - wave life - cycle behavior. *Quart. J. Roy. Meteor. Soc.*, **119**(509), 17–55, https://doi.org/10.1002/

qj.49711950903.

Wheeler, M., and G. N. Kiladis, 1999: Convectively coupled equatorial waves: Analysis of clouds and temperature in the wavenumber-frequency domain. *J. Atmos. Sci*., **56**(3), 374–399, https://doi.org/10.1175/1520-0469(1999)056<0374:CCEWAO>2.0.CO;2.

Wheeler, M. C., and H. H. Hendon, 2004: An all-season real-time multivariate MJO index: Development of an index for monitoring and prediction. *Mon. Wea. Rev*., **132**(8), 1917–1932, https://doi.org/10.1175/1520-0493(2004)132<1917:AARMMI>2.0.CO;2.

Yang, L., X. Wang, K. Huang, and D. X. Wang, 2015: Anomalous tropical cyclone activity in the Western North Pacific in August 2014. *Bull. Amer. Meteor. Soc*., **96**(12), S120-S125, https://doi.org/10.1175/BAMS-D-15-00125.1.

Zhang, G., Z. Wang, T. J. Dunkerton, M. S. Peng, G. Magnusdottir, 2016: Extratropical impacts on Atlantic tropical cyclone activity. *J. Atmos. Sci*., **73**(3), 1401–1418, https://doi.org/10.1175/JAS-D-15-0154.1.

Zhang, G., Z. Wang, M. S. Peng, and G. Magnusdottir, 2017: Characteristics and impacts of extratropical rossby wave breaking during the Atlantic hurricane season. *J. Climate*, **30**(7), 2363–2379, https://doi.org/10.1175/JCLI-D-16-0425.1.